JACS
JOURNAL OF THE AMERICAN CHEMICAL SOCIETY
pubs.acs.org/JACS
Article

Computationally Aided Design of Ionizable Cholesteryl Lipids for Lipid Nanoparticles to Modulate Hepatic mRNA Accumulation

Yilong Teng,[#] Yuxuan Guo,[#] Zhixiang Liu, Maoping Tang, William Stewart, Xiaoyang Xu,[*] and Xue-Qing Zhang[*]

Cite This: https://doi.org/10.1021/jacs.5c14870
Read Online

ABSTRACT: mRNA therapeutics are emerging as a revolutionary therapeutic modality, providing a versatile platform for the treatment and prevention of a broad spectrum of diseases. Nonviral nanoparticle-based delivery systems, particularly lipid nanoparticles (LNPs), are essential for their successful clinical translation. However, the currently FDA-approved four-component lipid nanoparticle (LNP) formulations primarily accumulate in the liver due to apolipoprotein E/Low-Density Lipoprotein Receptor (ApoE/LDLR)-mediated uptake by hepatic cells following systemic administration, which significantly limits extrahepatic mRNA delivery and restricts its broader therapeutic applications. Herein, we present a computationally assisted design approach to identify and optimize ionizable cholesteryl (iChol) lipids with extrahepatic delivery properties while formulating a three-component LNP system. Using DiffDock-L-assisted design, we rationally integrated two key components of LNPs, cholesterol and ionizable lipid, into a single chemical entity and developed a novel class of ionizable cholesteryl (iChol) lipids that exhibit attenuated interactions with ApoE. These iChol lipids, along with phospholipids and PEGylated lipids, can self-assemble into stable three-component lipid nanoparticles (Tc-LNPs). The Tc-LNPs exhibit decreased ApoE adsorption compared to conventional four-component LNP counterparts. Importantly, the Tc-LNPs show reduced hepatic accumulation via modulating ApoE/LDLR-mediated endocytosis in hepatocytes and improved spleen enrichment compared to commercially available LNPs. Additionally, this approach is applicable to other ionizable lipids, including the commercially available ALC-0315 lipid, paving a new way for accelerating the development of extrahepatic delivery LNPs and potentially expanding the applications of mRNA-based therapeutics.

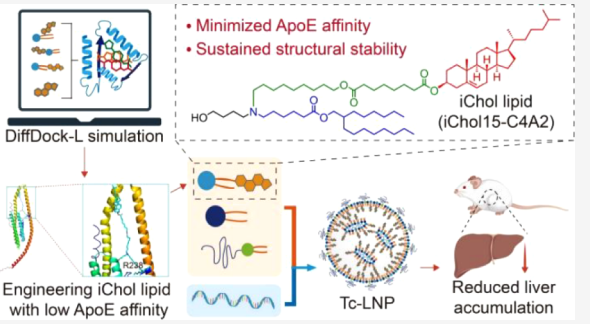

INTRODUCTION

mRNA therapeutics are emerging as a groundbreaking modality, offering a versatile platform for the treatment and prevention of various diseases.[1−7] Lipid nanoparticles (LNPs) serve as a pivotal platform for mRNA encapsulation and delivery, playing a crucial role in the clinical translation of mRNA-based therapeutics.[8,9] Their effectiveness has been exemplified by the remarkable success of FDA-approved COVID-19 mRNA vaccines (BNT162b2, mRNA-1273).[10,11] However, the current four-component lipid nanoparticle (LNP) formulations (ionizable lipid, cholesterol, phospholipid, and PEGylated lipid) tend to adsorb apolipoprotein E (ApoE) on their surface via cholesterol/ApoE interaction, facilitating LNPs internalization through ApoE/low-density lipoprotein receptor (LDLR)-mediated endocytosis.[12−16] This process enhances their preferential uptake by LDLR-rich hepatic cells, resulting in significant hepatic accumulation following systemic administration.[14,17,18] The inherent liver tropism of LNPs constrains the therapeutic applications of mRNA, restricting their use primarily to vaccine development and the treatment of hepatic disorders while limiting their potential for targeting nonhepatic organs.[19,20] Therefore, there is an unmet need for the development of novel strategies to effectively reduce hepatic accumulation and enhance extrahepatic mRNA delivery, thereby broadening the therapeutic potential of mRNA-based therapies and addressing unmet clinical challenges.

Herein, we propose a computation-assisted molecular design approach to synthesize, identify, and optimize lipids, and to develop three-component LNP (Tc-LNP) formulations with minimized adsorption of ApoE, aiming to reduce liver accumulation and enhance extrahepatic mRNA delivery. We computationally design a novel class of ionizable cholesteryl (termed iChol) lipids by structurally merging cholesterol and ionizable lipid components with the assistance of DiffDock-L

Received: August 26, 2025
Revised: October 3, 2025
Accepted: October 6, 2025

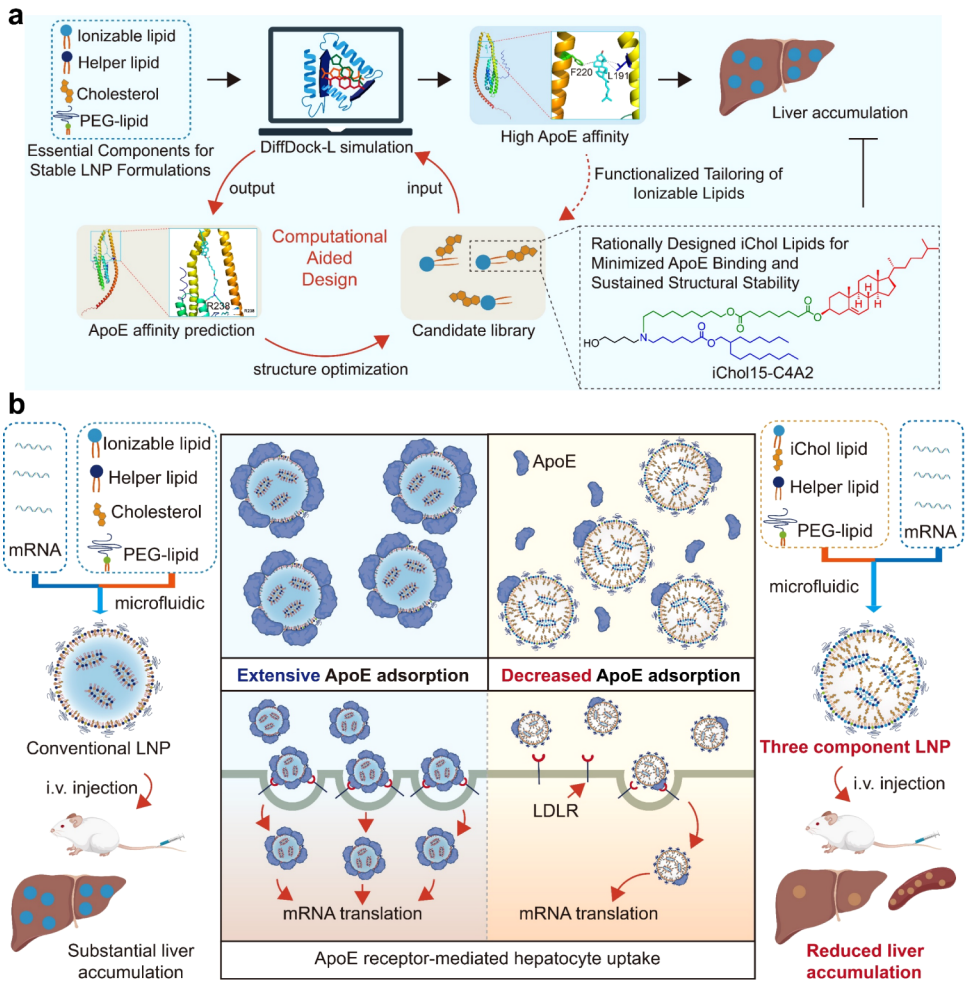

Figure 1. Schematic illustration of iChol lipid design and extrahepatic delivery mechanism of iChol lipid-based three-component lipid nanoparticles (Tc-LNPs). a, Computational docking simulations guided the rational design and optimization of the iChol lipid, achieving sustained structural stability, reduced ApoE binding, and ultimately minimized hepatic accumulation. b, Mechanism of extrahepatic mRNA delivery by Tc-LNPs. The iChol lipid, in combination with a helper lipid and a PEGylated lipid, self-assemble to form Tc-LNPs. Following intravenous administration, the Tc-LNPs exhibit reduced ApoE adsorption compared with conventional LNPs, resulting in enhanced extrahepatic delivery (e.g., spleen targeting).

molecular docking (Figure 1a). We hypothesize that DiffDock-L-assisted molecular binding simulations can rationally guide the design of functional iChol lipid molecules with reduced ApoE interaction, enabling high-throughput screening while minimizing the need for tedious wet lab chemical synthesis. The dual-functional properties of ionizable lipids and cholesterol are combined in the iChol lipids, by integrating the structural advantages of two key components in the LNP delivery system, iChol lipids retain the charge functionality of ionizable lipids for mRNA encapsulation and the structural stability provided by cholesterol. We further hypothesize that this "two-in-one" approach simplifies LNP formulations and facilitates large-scale manufacturing. More importantly, the Tc-LNP system can effectively reduce ApoE adsorption on the nanoparticle surface, thereby decreasing LDL receptor-mediated hepatic cellular uptake, reducing liver accumulation, and facilitating targeting of extrahepatic organs (Figure 1b).

DiffDock-L is a computational method that leverages the calculation of physicochemical parameters, such as van der Waals interactions, electrostatic forces, and solvation effects, to predict molecular binding affinity and binding conformation.[21] In this study, we utilize DiffDock-L to assess the binding affinity and conformational states of ApoE in complex with cholesterol, while also analyzing the specific binding site involved in their interaction. Based on the simulation results, we modified the chemical structure of cholesterol to alter its conformation, with the goal of reducing or blocking the cholesterol-ApoE interaction. Furthermore, we incorporated an ionizable amine moiety and hydrophobic alkyl chain into the cholesterol backbone to synthesize iChol lipids, thereby integrating the functionalities of cholesterol and ionizable lipids into a singular chemical entity. The resulting iChol lipids feature three key structural components: (1) a hydrophilic, ionizable headgroup, (2) a biodegradable alkyl chain tail that promotes biosafety and cellular uptake,[16,22] and (3) a terminal cholesterol moiety covalently conjugated to the alkyl chain to enhance LNP stability. A library of the 105 novel lipids was systematically designed, and the interactions between the lipids and ApoE were simulated using DiffDock-L. The simulating revealed that all the designed iChol lipids exhibited comparatively weaker interactions with ApoE than cholesterol. We then synthesized iChol lipids through nucleophilic substitution reactions between amine intermediates and alkyl bromides to validate the simulation and evaluate transfection efficiency. When combined with phospholipids and PEGylated lipids (DMG-PEG2000), these iChol lipids self-assembled into

https://doi.org/10.1021/jacs.5c14870
J. Am. Chem. Soc. XXXX, XXX, XXX−XXX

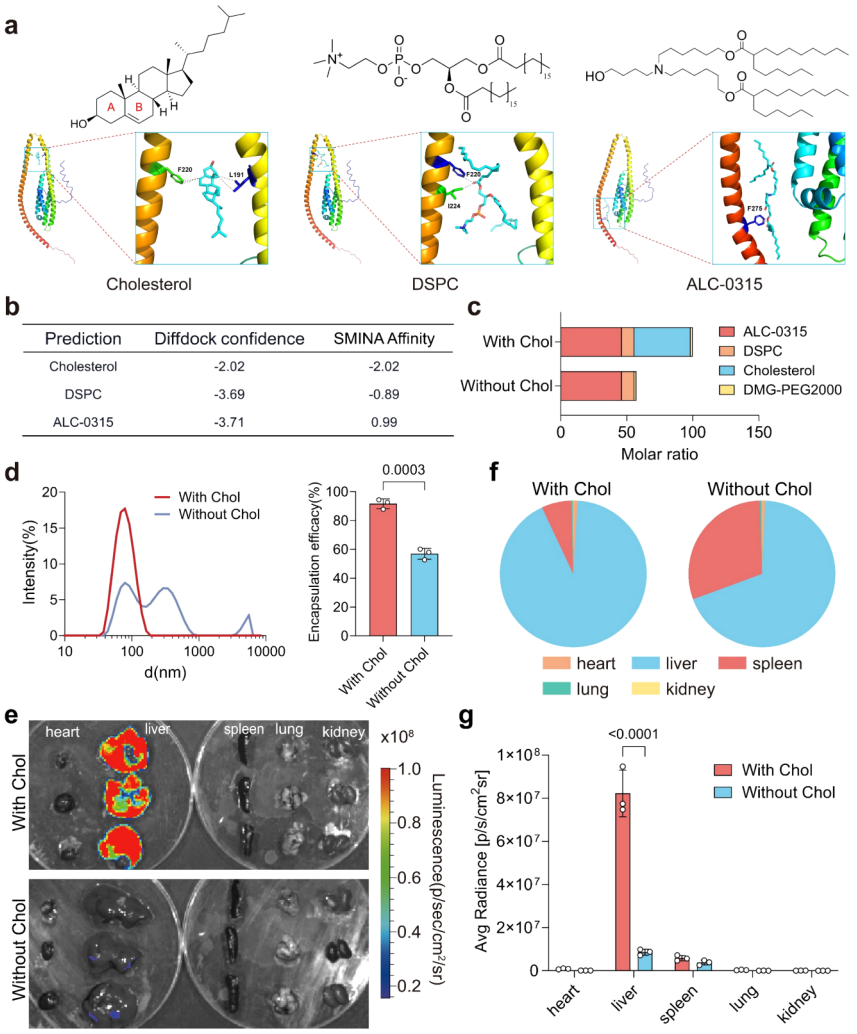

Figure 2. Cholesterol removal attenuates hepatic accumulation of LNPs. a, Structural representations and predicted binding poses of cholesterol, DSPC and ALC-0315 at the interfaces of ApoE, as predicted by DiffDock-L molecular docking simulations. b, The top-ranked docking result predicted by DiffDock-L. Lower affinity values (more negative) indicate stronger binding between the lipid and ApoE, reflecting a more favorable interaction. c, The formulation of four-component ALC-0315 based LNPs (with cholesterol, ALC-0315 LNPs) and three-component ALC-0315 based LNPs (without cholesterol). d, Hydrodynamic diameter and encapsulation efficiency of ALC-0315 LNP formulated with or without cholesterol. e, Bioluminescence IVIS images of major organs at 6 h post intravenous administration of ALC-0315 LNPs formulated with or without cholesterol. Balb/c mice were intravenously administrated with LNPs encapsulating luciferase mRNA (0.2 mg/kg, n = 3). f, Normalized bioluminescence ratio in major organs quantified by IVIS imaging. g, Quantification of average bioluminescence intensity by IVIS imaging, indicating the luciferase expression in major organs. Data are expressed as mean ± standard deviation (SD). The average value of 3 samples in each group was analyzed in f. Statistical significance in d and g was calculated using unpaired t test.

Tc-LNPs via microfluidic mixing, demonstrating high mRNA encapsulation efficiency and superior stability. We performed structure−activity relationship (SAR) analysis on the 105 lipids library through systematic in vitro screening, and identified ten lead compounds that markedly reduced hepatic accumulation while enabling observable mRNA delivery to extrahepatic tissues (particularly the spleen) following intravenous administration. Among the identified lipids, seven iChol-based Tc-LNPs achieved comparable or superior transfection efficiency to conventional LNPs (ALC-0315 or Dlin-MC3-DMA-based LNPs, termed ALC-0315 LNPs or MC3 LNPs) following intramuscular administration. Further research revealed that Tc-LNPs displayed reduced ApoE adsorption compared to conventional LNPs and were less influenced by ApoE/LDLR-mediated cellular uptake. Proteomics analysis revealed that Tc-LNPs exhibited up to 90% reduced ApoE protein adsorption compared to conventional LNPs. These results validate our computational predictions, confirming that iChol lipids effectively reduce hepatic accumulation while promoting mRNA delivery to extrahepatic tissues (spleen tropism). It is worth noting this computation-assisted "two-in-one" strategy can be adapted for commercial lipids derivatization, including ALC-0315. For example, we synthesized two cholesterol-modified ALC-0315 variants by replacing the 2-hexyl decanoate tail with cholesterol, both producing enhanced mRNA transfection efficacy to the spleen compared to the parent compound (liver tropism).

Collectively, our study demonstrates that computational aided rational design of iChol lipids enables precise modulation of LNP protein adsorption, thereby reducing hepatic accumulation while enhancing mRNA delivery to nonhepatic tissues, further highlights the advantages and promise of the computation-assisted molecular design strategy for lipid-based platforms with improved extrahepatic mRNA

https://doi.org/10.1021/jacs.5c14870
J. Am. Chem. Soc. XXXX, XXX, XXX−XXX

delivery capabilities. This innovative approach has the potential to broaden the scope of molecular design for mRNA delivery vehicles, simultaneously addressing the clinical challenge of extrahepatic mRNA-based therapies.

RESULTS

Cholesterol Depletion Attenuates Hepatic Accumulation of LNPs. Given the pivotal role of ApoE-LNP interactions in mediating hepatic accumulation of LNPs,[12,23,24] we performed molecular docking of the three main components of the commercially available LNP, cholesterol, DSPC, and ALC-0315, with ApoE (Figure 2a). The computational analyses were conducted using DiffDock-L, an enhanced deep learning-based molecular docking platform.[25−27] The binding affinity values were −2.02, −0.89, and 0.99 for cholesterol, 1,2-distearoyl-*sn*-glycero-3-phosphocholine (DSPC), and ALC-0315, respectively (Figure 2b). Lower affinity values (more negative) indicate stronger binding between the lipid and ApoE, reflecting a more favorable interaction. The results suggest that cholesterol possesses the highest affinity for ApoE, and the possible binding sites are in the A and B rings of cholesterol (Figure 2a). Then, cholesterol was removed from the ALC-0315 LNPs formulation in an attempt to reduce the interaction between LNP and ApoE, with the modified formulation depicted in Figure 2c. Cholesterol elimination induced significant physicochemical destabilization, manifested as a 216% increase in hydrodynamic diameter (76.6 to 241.3 nm), 87% elevation in polydispersity index (PDI: 0.135 to 0.252), and 30% reduction in encapsulation efficiency (89.7% to 60.1%) (Figure 2d). Cholesterol serves as a critical determinant of LNP structural integrity.[28] And cholesterol ablation from ALC-0315 LNPs caused a 24% reduction in hepatic accumulation compared to LNPs that retained cholesterol (Figure 2e,f), which is in line with previous study.[29] These findings are consistent with the simulation, indicating that cholesterol is critical role in liver accumulation of LNPs. It is worth mentioning that the mRNA transfection efficacy, as measured by luminescence intensity, declined by an order of magnitude (Figure 2e,g). The results reveal that cholesterol removal reduces the liver accumulation of LNPs, and cholesterol is critical for stabilizing LNPs, optimizing encapsulation efficiency, and enhancing transfection efficacy. Therefore, we propose dual-functional cholesterol-ionizable lipid hybrids for the development of Tc-LNPs. The yielding lipid hybrids retain cholesterol fragments to enhance stability of the Tc-LNPs while minimizing free cholesterol-ApoE interactions, thereby reducing hepatic accumulation.

Molecular Docking-Guided Design and Synthesis of iChol Lipids for Tc-LNPs. Ionizable lipids are small-molecule amphiphiles with a hydrophilic head typically containing an ionizable amino group, and two (or more) hydrophobic alkyl tails.[6] In clinically approved LNP formulations like Parisian (Onpattro), the molar ratio of ionizable lipids to cholesterol is typically about 1:1.[6,30] Accordingly, we engineered novel ionizable lipids, one cholesterol fragment is covalently linked to an ionizable lipid via the hydroxyl group of the A-ring of cholesterol, aiming to sterically hinder cholesterol-ApoE recognition processes. Three ionizable lipids with systematically varied structural configurations were designed (Figure S1), featuring covalent anchoring of cholesterol moieties at distinct sites: headgroup proximity (**Compound 1D**), midtail integration (**Compound 2D**), and terminal alkyl chain modification (**Compound 3D**). The binding affinities of the iChol-lipids to ApoE were quantified by computing the free energy change of their molecular interactions using DiffDock-L, revealing the affinity values of −1.77 for **Compound 1D**, 15.44 for **Compound 2D**, and 68.98 for **Compound 3D** (Table S1). This result indicates that **Compound 3D** has the weakest binding affinity to ApoE among the tested lipids. While cholesterol incorporation at the headgroup of the ionizable lipid modulates the hydrophilic−lipophilic balance, midtail integration introduces synthetic complexity that compromise high-throughput screening efficiency. Consequently, we adopted a terminal-tail cholesterol conjugation strategy to optimize both molecular functionality and synthetic accessibility. Furthermore, to simultaneously enhance mRNA transfection efficacy and improve the biosafety profile of LNPs, we deliberately incorporated an additional ester bond into the alkyl chain architecture of the cholesterol moiety.[16,22]

Subsequently, we designed the brominated alkyl intermediate library with a cholesterol fragment and two ester bonds, constituting one tail segment of the newly designed ionizable iChol lipid (Figure 3a). To systematically evaluate the SAR between cholesterol alkyl chain length and LNP performance, we designed a series of cholesterol derivatives with alkyl chains varying from C6 to C18 to assess their effects on ApoE binding affinity and mRNA delivery efficacy (Figure 3b, cholesterol tail). The series comprised Chol6, Chol10, Chol12, Chol13, Chol14, Chol15, and Chol18, where the prefix "Chol" denotes cholesterol, and the numeric suffix indicates the alkyl chain length (C6−C18). The ionizable amine headgroup and the other alkyl tail segment constitute the secondary amine intermediate library of the iChol lipid (Figure 3c). The intermediate features a hydroxyl-functionalized amino headgroup, incorporating three distinct polar moieties (ethanol, butanol, and diethylene glycol fragments), respectively. Under acidic conditions, protonation of the amino group promotes mRNA complexation through electrostatic interactions, while the hydroxyl moieties in the headgroup further enhance mRNA binding via hydrogen bonding. This dual-interaction mechanism facilitates efficient mRNA encapsulation by ionizable lipids. The other alkyl tail segment was linked to the amino group, comprising both linear (C6−C9) and branched (C10−C18) alkyl chain. Structurally diverse linkers (including ester, carbamate, *N*-methyl carbamate, and acetal bonds) were incorporated within the alkyl chains to bridge linear and branched segments, enabling biodegradability optimization. Ultimately, we designed 15 secondary amine intermediates to assess the impact of structural segment on transfection efficiency of lipids, thereby enabling SAR analysis. In the secondary amine intermediate nomenclature, "C" represents the alkyl carbon chain linking the hydroxyl and ionizable amino groups, with the following numeral indicating chain length, while "O" denotes oxygen-containing moieties. "A" denotes the amino group, with subsequent numerals (**1**-**4**) indicating specific hydrophobic alkyl chain combinations: **1** (linear C6 and branched C15), **2** (linear C5 and branched C16), **3** (linear C7 and branched C16), and **4** (linear C9 and branched C11). The letter following "A" indicate the linkage type: "C" (carbamate), "CM" (methylated carbamate), or "Ac" (acetal), characterizing the structural features of the secondary amine intermediate. Through rational molecular design, we developed structurally optimized intermediates that constitute a novel class of ionizable lipids.

Using combinatorial chemistry with the rationally designed intermediates, we generated a library of 105 structurally diverse

https://doi.org/10.1021/jacs.5c14870
J. Am. Chem. Soc. XXXX, XXX, XXX−XXX

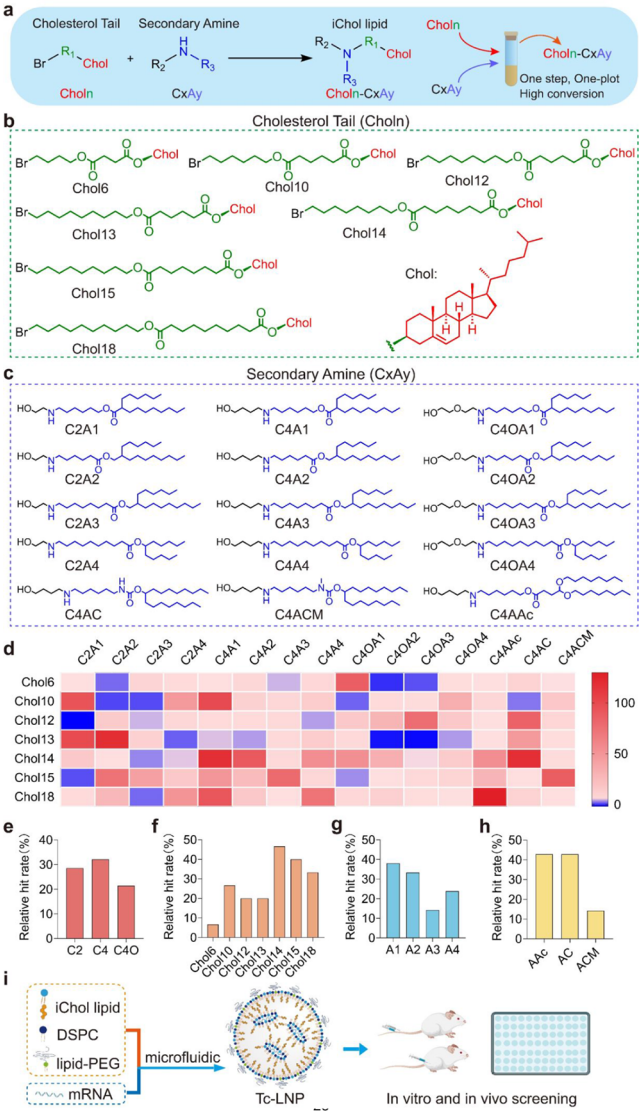

Figure 3. Molecular docking-guided design and synthesis of iChol lipids for Tc-LNPs. a, Schematic structure and synthesis of iChol lipids using cholesterol tails and secondary amine intermediates with high conversion, enabling fast and efficient production. b, c, Chemical structure of cholesterol tails (b) and secondary amines (c) designed for ionizable cholesteryl (iChol) lipids. d, Affinity values between iChol lipids and ApoE predicted by DiffDock-L. Red indicates affinity values greater than 0, while blue represents affinity values less than 0. Lower affinity values (more negative) indicate stronger binding ability. e−h, Structure−activity (affinity) relationships (SAR) of iChol lipids headgroup with different chains between hydroxyl group and amino group (e), length of cholesterol tails (f), secondary amine intermediate (g), and secondary amine intermediates featuring carbamate, methylated carbamate, and acetal linked, respectively (h). The hit rate (%), calculated as the proportion of active lipids (affinity values >22.66, the average threshold) among all selected lipids. i, Schematic illustration of the formulation and screening process for Tc-LNPs.

iChol lipids. The binding affinities of iChol lipids for ApoE were calculated using DiffDock-L (Figure 3d). The results revealed that >80% of the lipid library (represented by red tiles) formed less stable complexes with ApoE compared to cholesterol and DSPC, as evidenced by their positive binding affinity values. The hit rate (%), calculated as the proportion of active lipids (affinity values >22.66, the average threshold) among all selected lipids, was employed to quantify the relative performance of key iChol lipid structural fragments and establish structure-affinity relationships. Headgroup engineering modulated ApoE binding, where oxygen incorporation in the diethylene glycol fragment (C4O, 21.4% hit rates) spacer enhanced affinity relative to the butanol (C4, 32.1% hit rates) and the ethanol (C2, 28.6% hit rates) variant chain (Figure 3e). Notably, iChol lipids displayed progressively decreasing affinity with increasing cholesterol tail length, with Chol6 having the highest affinity, followed by Chol15 and Chol18, while Chol14 exhibited the lowest affinity (Figure 3f). Among amine intermediates, iChol lipids incorporating A3 (linear C7 and branched C16) showed the highest affinity, while those with A1 (linear C6 and branched C15), AC (carbamate-linked), or AAc (acetal-linked) structural segments had lower binding (Figure 3g,h). The majority of designed iChol lipids demonstrates limited ApoE binding. Structural analysis revealed that Chol14 tails, C4 headgroups, and A1/AC/AAc amine moieties were particularly effective in attenuating ApoE binding affinity.

While molecular simulations can predict the iChol lipid-ApoE binding affinities, experimental validation is crucial for identifying optimal mRNA transfection performance. We therefore synthesized all designed intermediates for subsequent iChol lipids preparation. The synthetic procedures and characterization data (including NMR and mass spectrometry) for all intermediates are provided in the Supporting Information (Schemes S1−S14 and Figures S2−S34). The iChol lipids were synthesized through a one-pot nucleophilic substitution reaction between brominated cholesterol alkyl (cholesterol tail) and secondary amine, using potassium carbonate as an acid scavenger (Figure 3a). Subsequently, the reaction mixture was filtered and concentrated to afford the crude product. The representative lipid **iChol15-C4A2** achieved 94.1% purity as verified by HPLC-MS and TLC (HPLC-MS, TLC, Figures S35, S36 and Table S2), eliminating the requirement for further purification. After synthesizing all 105 iChol lipids, we prepared Tc-LNPs using microfluidic technology to evaluate their transfection efficacy and SAR in vitro and in vivo (Figure 3i), targeting iChol lipids for high-efficiency extrahepatic mRNA delivery. In summary, we designed and synthesized 105 structurally diverse iChol lipids using a simple and efficient method, and their bioactivity will be further investigated.

In Vitro mRNA Delivery by Tc-LNPs and SAR Study of iChol Lipids. Tc-LNP-mediated mRNA transfection efficacy was quantitatively assessed in HEK293 cells using luciferase-based bioluminescence. Luciferase mRNA was encapsulated in Tc-LNPs (iChol lipid: DSPC: DMG-PEG2000 = 50:50:1.5 molar ratio) via microfluidic mixing.[31] Tc-LNPs exhibited high encapsulation efficiency (>80%), with a favorable particle size distribution ranging from 80 to 120 nm, and low polydispersity index (PDI < 0.25, typically <0.15) (Table S3). The in vitro screening results of Tc-LNP-mediated mRNA transfection efficiency are presented in the heatmap (Figure 4a). Based on these data, we calculated the hit rate (%), defined as the percentage of active lipids (luminescence intensity >7291.8 RLU, mean threshold) among the total selected lipids, to evaluate key iChol lipid structural fragments and establish SAR. Butanol (C4) and diethylene glycol (C4O) fragments showed comparable performance (35.7% vs 39.3%), both significantly surpassing the ethanol fragments (C2, < 10%) (Figure 4b). The Chol13 and Chol15 cholesterol tail fragments demon-

https://doi.org/10.1021/jacs.5c14870
J. Am. Chem. Soc. XXXX, XXX, XXX−XXX

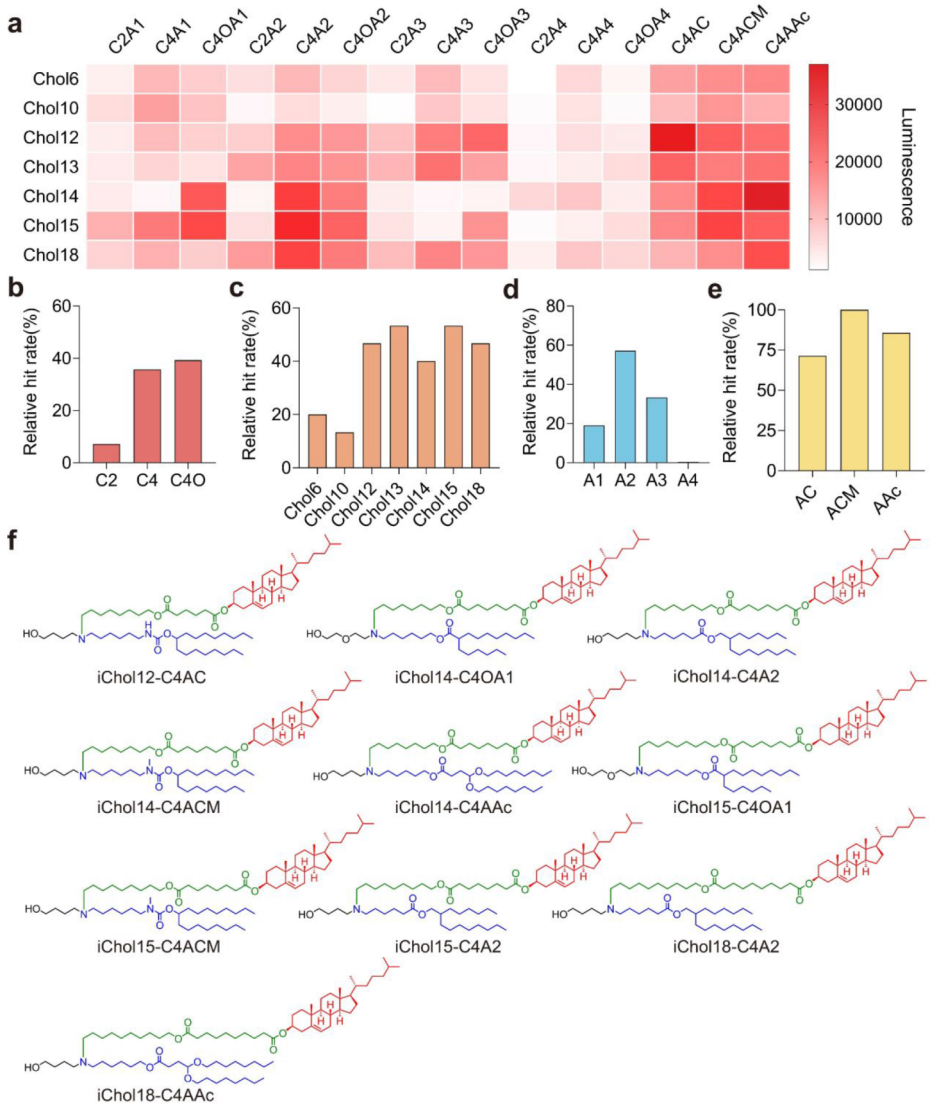

Figure 4. mRNA delivery in vitro by Tc-LNPs and SAR study of iChol lipids. a, The heatmap of in vitro screening of Tc-LNP-mediated luciferase mRNA transfection in HEK293 cells (25 ng luciferase mRNA per well in 96-well plate, $n = 3$). b−e, SAR of iChol lipids headgroup with different chains between hydroxyl group and amino group (b), length of cholesterol tails (c), secondary amine intermediate (d), secondary amine intermediates featuring carbamate, methylated carbamate, and acetal linked, respectively (e). The hit rate (%) was defined as the percentage of active lipids (luminescence intensity >7291.8 RLU, mean threshold) among the total selected lipids. f, The chemical structures of 10 top-performing iChol lipids.

strated significantly higher transfection efficacy than other cholesterol tails (Figure 4c). In the hydrophobic alkyl tail, incorporation of 2-hexyldecanol fragments (such as A2, linear C5 and branched C16) enhances the mRNA transfection efficacy of the iChol lipids (Figure 4d). Carbamate, *N*-methylcarbamate, and acetal linkers in the lipid backbone boosted mRNA delivery performance (Figure 4e). The top ten iChol lipids with the best cell-level performance were identified, as shown in Figure 4f. Structural analysis revealed that the lead lipids predominantly incorporated butanol ($n = 8$) and ethylene glycol ($n = 2$) headgroups, featured Chol14/Chol15 cholesterol tails, and ester/*N*-methylcarbamate/acetal linkers. The ten iChol lipids were synthesized, purified (Scheme S15), and characterized by NMR/MS (Figures S37−S46). And, they showed no obvious cytotoxicity (Figure S47), suggesting favorable safety profiles of iChol lipids. In summary, we developed a simplified lipid nanoparticle system (Tc-LNPs) based on iChol lipids, systematically elucidated their SAR in vitro, and identified ten lead lipids with both high efficiency and excellent safety profiles. The identified lipids were selected for subsequent in vivo validation.

Tc-LNP-Mediated mRNA Delivery In Vivo. The ten lead lipids were evaluated for in vivo mRNA delivery efficacy by quantitative bioluminescence imaging. Ten luciferase mRNA-loaded Tc-LNPs prepared via the established protocol exhibited high encapsulation efficiency (mostly >90%), 80−120 nm particle size, low PDI (PDI < 0.15), and a near-neutral zeta potential (−1 to −2 mV) (Figure S48). Following intramuscular injection, the seven iChol-based Tc-LNPs exhibited comparable or significantly higher transfection efficiency at the injection site than commercial carriers, including ALC-0315 and MC3 LNPs. Intriguingly, **iChol15-C4A2** and **iChol15-C4ACM**-based Tc-LNPs (**iChol15-C4A2** Tc-LNPs and **iChol15-C4ACM** Tc-LNPs) demonstrated the most superior mRNA delivery efficacy in vivo, as shown in Figure 5a,b. In addition, Tc-LNPs exhibited remarkably

https://doi.org/10.1021/jacs.5c14870
J. Am. Chem. Soc. XXXX, XXX, XXX−XXX

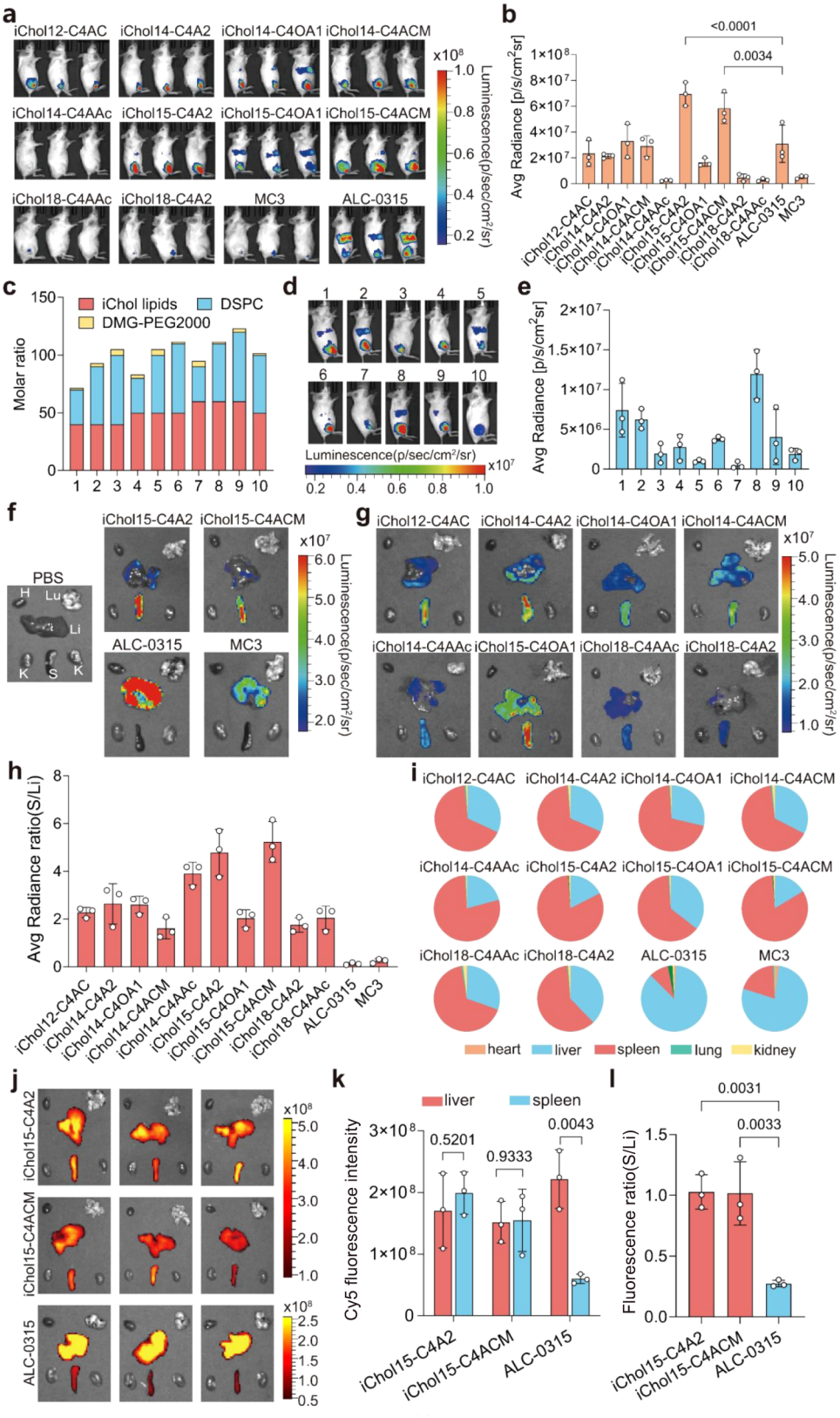

Figure 5. Tc-LNP-mediated mRNA delivery in vivo. a, In vivo mRNA delivery of top 10 Tc-LNPs following intramuscular administration, measured by IVIS, MC3 and ALC-0315 were used as controls (5 μg luciferase mRNA per mouse, n = 3). b, Quantification of average bioluminescence intensity of the injection site by IVIS imaging based on a at 6 h post-treatment. c, Formulation optimization design. d, e, In vivo mRNA delivery of the designed 10 formulations following intramuscular administration (1 μg per mouse, n = 3), measured by IVIS. (d), Quantification of average bioluminescence intensity of the injection site by IVIS imaging based on d at 6 h post-treatment (e). In vivo mRNA delivery of top two Tc-LNPs (f) and the remaining eight optimal Tc-LNPs (g) following intravenous administration (0.1 mg/kg, n = 3). MC3 and ALC-0315 LNPs were used as controls. Representative IVIS images of major organs 6 h post-treatment were presented. H: heart, Lu: lung, Li: liver,

https://doi.org/10.1021/jacs.5c14870
J. Am. Chem. Soc. XXXX, XXX, XXX−XXX

Figure 5. continued

S: spleen K: kidney. h, The bioluminescence ratio of spleen to liver. i, Pie chart analysis of luciferase expression in major organs based on bioluminescence imaging depicted in f and g. Data represent the average bioluminescence intensity from three samples per group. j, In vivo biodistribution of Tc-LNPs following intravenous administration. Each mouse received an intravenous administration of ^{Cy5}mRNA at a dose of 0.3 mg/kg (n = 3). k, Fluorescence quantification analysis of liver and spleen. l, Fluorescence ratio of spleen to liver. Data are expressed as mean ± SD. Statistical significance in b and l was analyzed using one-way ANOVA with Dunnett's multiple comparisons test. Statistical significance in k was analyzed using unpaired t test.

reduced hepatic luciferase expression compared to the ALC-0315 LNP which induced robust hepatic luciferase expression (Figure 5a). Notably, **iChol12-C4AC** and **iChol14-C4AAc** Tc-LNPs exhibited the best performance in vitro. The in vivo delivery efficacy of Tc-LNPs did not show a complete correlation with the in vitro results, which is in line with previous findings.[32−34] This poor correlation may be partly attributed to the complex in vivo environment, where protein adsorption onto LNP surfaces could significantly alter their biological behavior. Tc-LNPs achieved excellent transfection efficacy and potentially reducing hepatic mRNA delivery following intramuscular administration.

We then optimized the Tc-LNP formulations based on the lipid **iChol15-C4A2**, yielding ten **iChol15-C4A2** Tc-LNPs with the following compositional ranges: iChol lipids (40−60 molar ratio), DSPC (30−60 molar ratio), and DMG-PEG2000 (1.5−5 molar ratio) (Figure 5c), the physicochemical characterization of LNPs was presented in Figure S49. Following intramuscular injection, Formulation 8 achieved superior mRNA delivery efficiency, along with favorable physicochemical properties (hydrodynamic diameter: 106 nm, PDI: 0.09, encapsulation efficiency: 94.7%) (Figures S49 and 5d,e). Based on the obtained results, Formulation 8 was chosen to prepare Tc-LNPs, each incorporating a single one of the 10 selected lipids, for in vivo biodistribution analysis following intravenous injection. Tc-LNPs showed reduced hepatic mRNA expression but enhanced splenic expression compared to MC3 and ALC-0315 LNPs (Figures 5f,g and S50). **iChol15-C4A2** Tc-LNPs and **iChol15-C4ACM** Tc-LNPs mediated the highest splenic mRNA transfection efficacy in vivo (Figure 5h). The spleen-to-liver luminescence intensity ratios for **iChol15-C4A2** and **iChol15-C4ACM** Tc-LNPs were 4.78 and 5.20, respectively, representing a 20−50-fold increases compared to MC3 (0.24) and ALC-0315 (0.12) LNPs (Figure 5h). DiffDock-L predictions revealed that iChol lipids exhibit reduced ApoE binding affinity, which correlated with their extrahepatic tropism (Table S4 and Figure 5h,i). This validated our computational design strategy and enabled rational engineering of iChol lipids to minimize hepatic mRNA delivery while enhancing spleen-specific tropism, achieving markedly improved splenic mRNA delivery efficiency.

We further evaluated Tc-LNP biodistribution by intravenous administration of Cy5-labeled mRNA (^{Cy5}mRNA)-loaded Tc-LNPs. The **iChol15-C4A2** Tc-LNP group exhibited a 5-fold higher spleen-to-liver fluorescence intensity ratio (1.0 vs 0.2) compared to ALC-0315 LNP, demonstrating preferential splenic accumulation of Tc-LNPs (Figure 5j,−l). The variations between luciferase expression (50-fold increase) and LNP biodistribution (5-fold increase) may stem from differences in analytical methods, and the liver's sinusoidal architecture promoting nanoparticle uptake by hepatic sinusoidal endothelial cells and Kupffer cells.[20,35,36] Tc-LNPs demonstrated superior in vivo mRNA transfection efficiency and enhanced extrahepatic accumulation compared to conventional LNPs. Notably, **iChol15-C4A2**- and **iChol15-C4ACM**-containing Tc-LNPs exhibited particularly promising performance and were consequently selected for subsequent studies.

Extrahepatic mRNA Delivery Mechanism of Tc-LNPs. We hypothesize that rationally designed iChol lipids with attenuated ApoE interactions will generate Tc-LNPs that exhibit reduced ApoE adsorption capacity and consequently demonstrate decreased dependence on ApoE/LDLR-mediated cellular uptake and mRNA delivery. In this context, we evaluated the role of ApoE-LDLR interaction in regulating Tc-LNP-mediated mRNA delivery. ^{Cy5}mRNA-loaded LNPs formulated with ALC-0315, **iChol15-C4A2**, or **iChol15-C4ACM**, were preincubated with ApoE to facilitate protein corona formation. Cellular uptake studies in LDLR-expressing HepG2 cells revealed ApoE preincubation markedly enhanced ALC-0315 LNP uptake, while Tc-LNPs internalization remained unaffected (Figures 6a,b and S51). Similarly, luciferase expression assays revealed a concentration-dependent elevation in mRNA expression levels of HepG2 cells incubated with ApoE-treated ALC-0315 LNPs, while no significant change was observed in Tc-LNPs (Figure 6c). Furthermore, Tc-LNPs preincubated with ApoE demonstrated significantly lower transfection efficiency compared to ALC-0315 LNPs subjected to the same treatment (Figure 6c). Parallel experiments in LDLR-deficient HEK293 cells demonstrated that ApoE preincubation did not affect cellular uptake or luciferase expression for either ALC-0315 LNPs or Tc-LNPs (Figures 6d−f and S52).

To further elucidate the mechanism underlying the lack of responsiveness of Tc-LNPs to LDLR-mediated delivery to hepatocytes, we preincubated EGFP mRNA-loaded Tc-LNPs or ALC-0315 LNPs with ApoE, followed by incubation with HepG2 or HEK293 cells that had been pretreated with ApoE to competitively block surface LDLR. Cells treated with LNPs but without ApoE pretreatment served as controls (Figure S53a). In ApoE-pretreated HepG2 cells, the transfection efficiency of ApoE-preincubated ALC-0315 LNPs decreased by ∼80% compared to controls, whereas Tc-LNP-mediated transfection remained unaffected (Figure S53b). In contrast, neither ApoE-preincubated ALC-0315 LNPs nor Tc-LNPs showed altered transfection efficiency in ApoE-pretreated HEK293 cells (Figure S53c). Collectively, these results indicate that Tc-LNPs exhibit minimal dependence on ApoE/LDLR-mediated hepatocyte uptake and transfection compared to ALC-0315 LNPs. This effect is attributed to the diminished ApoE adsorption of Tc-LNPs relative to ALC-0315 LNPs.

The protein corona adsorbed onto LNPs is a critical determinant of their biodistribution. This is substantiated by the observation that ApoE adsorption promotes LDLR-mediated hepatic targeting of LNPs (e.g., ALC-0315 LNPs).[14,37] To characterize the protein corona composition adsorbed by Tc-LNPs, we incubated the LNPs with mouse plasma and analyzed the adsorbed proteins using liquid

https://doi.org/10.1021/jacs.5c14870
J. Am. Chem. Soc. XXXX, XXX, XXX−XXX

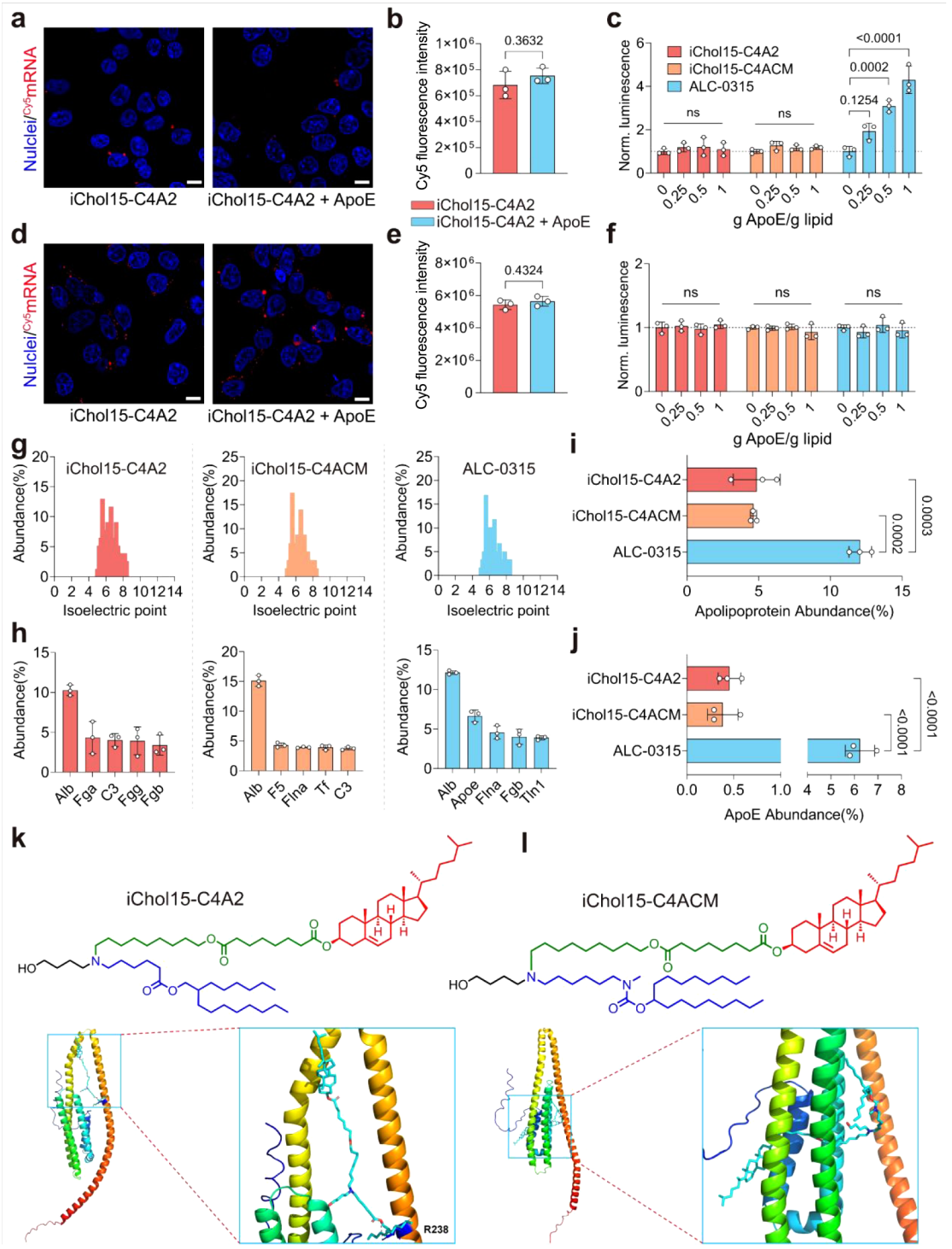

Figure 6. Mechanism of extrahepatic mRNA delivery facilitated by Tc-LNPs. a–f, ApoE/LDLR-mediated effects on cellular uptake and mRNA delivery in HepG2 (a–c) and HEK293 cells (d–f). a, Representative images showing the cellular uptake of ApoE unincubated or preincubated **iChol15-C4A2** Tc-LNP (1.0 g ApoE/g lipid) by HepG2 cells. Scale bar = 10 μm. b, Quantification of Cy5 fluorescence intensity in HepG2 cells treated with ApoE unincubated or preincubated **iChol15-C4A2** Tc-LNPs. c, Luciferase mRNA delivery to HepG2 cells by ApoE preincubated Tc-LNPs or ALC-0315 LNPs. d, Representative images illustrating the cellular uptake of ApoE unincubated or preincubated **iChol15-C4A2** Tc-LNPs in HEK293 cells. Scale bar = 10 μm. e, Quantification of Cy5 fluorescence intensity in HEK293 cells treated with ApoE unincubated or preincubated **iChol15-C4A2** Tc-LNPs. f, Luciferase mRNA delivery to HEK293 cells by ApoE preincubated Tc-LNPs or ALC-0315 LNPs. g, h, Isoelectric points distribution (g) and top five adsorbed proteins on Tc-LNPs or ALC-0315 LNPs (h). i, Apolipoprotein abundance of the protein corona on Tc-LNPs or ALC-0315 LNP. j, ApoE abundance of the protein corona on Tc-LNPs or ALC-0315 LNP. k, l, Schematic of the chemical structure of the **iChol15-C4A2** (k) and **iChol15-C4ACM** (l) and their interaction with ApoE. Data are expressed as mean ± SD. Statistical significance in b and e was determined using an unpaired *t* test. In c, f, h and j, statistical significance was analyzed by one-way ANOVA with Dunnett's multiple comparisons test.

https://doi.org/10.1021/jacs.5c14870
J. Am. Chem. Soc. XXXX, XXX, XXX−XXX

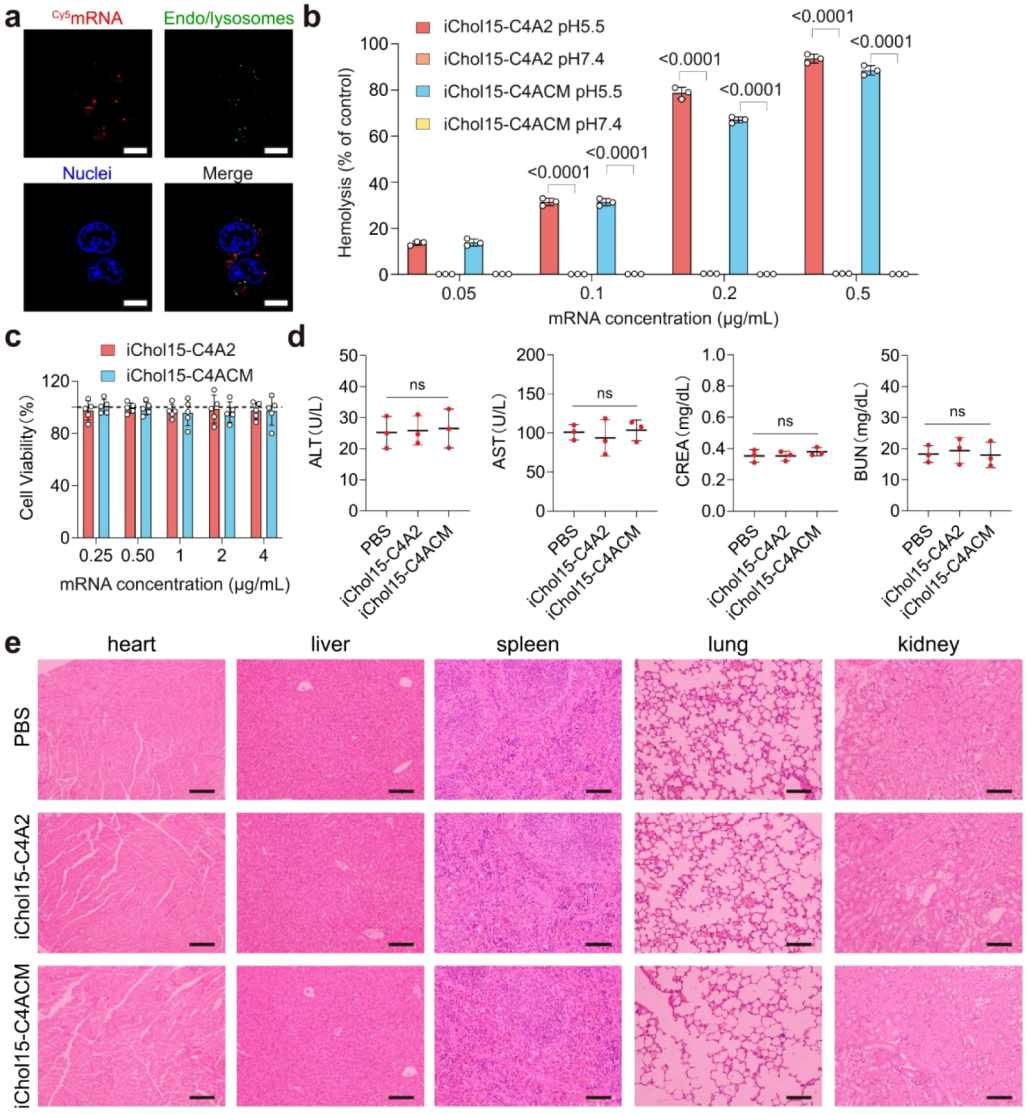

Figure 7. Endosomal Escape ability and biocompatibility of Tc-LNPs. a, Representative images of endosome escape of **iChol15-C4A2** Tc-LNPs. Scale bar = 10 μm. HEK293 cells in confocal culture dish were treated with 1 μg ^{Cy5}mRNA encapsulated in Tc-LNP. b, Hemolysis of Tc-LNPs at physiological and acidic conditions. c, Cytotoxicity of two Tc-LNPs at varying mRNA concentrations (n = 5). The dashed line indicates 100% cell viability. d, e, Biocompatibility evaluation of Tc-LNPs. Balb/c mice were administered Tc-LNPs intravenously at a mRNA dose of 0.5 mg/kg, or PBS (pH 7.4) as a negative control. d, Alanine aminotransferase (ALT), aspartate aminotransferase (AST), creatinine (CREA) and blood urea nitrogen (BUN) assays. e, H&E staining of major organs. Scale bar = 100 μm. Data are expressed as mean ± SD. Statistical significance in b was determined using an unpaired t test. In d, statistical significance was analyzed by one-way ANOVA with Dunnett's multiple comparisons test.

chromatography−mass spectrometry (LC-MS). As show in Figure 6g, both **iChol15-C4A2** and **iChol15-C4ACM** Tc-LNPs displayed isoelectric point distributions comparable to ALC-0315 LNPs. Quantitative analysis revealed similar albumin adsorption levels between these LNP formulations (Figure 6h). Notably, Tc-LNPs exhibited significantly reduced apolipoprotein adsorption (4.7% for Tc-LNPs vs 12.1% for ALC-0315 LNPs, Figure 6i). Most strikingly, Tc-LNPs exhibited minimal ApoE adsorption, with only 0.4% of the total protein corona consisting of ApoE. This represents a 90% reduction compared to ALC-0315 LNPs (6.2%) (Figure 6j and Tables S5−S7). The substantially reduced ApoE adsorption of Tc-LNPs directly contributes to the attenuated hepatocyte uptake and transfection efficiency.

Molecular dynamics simulation using the DiffDock—L algorithm was conducted to visualize the interaction interfaces between ApoE and the lipids (iChol lipids and cholesterol). The results indicated that the binding affinities between ApoE and iChol lipids (**iChol15-C4A2**: 24.47; **iChol15-C4ACM**: 87.34) were significantly weaker than those between ApoE and cholesterol (−2.02) (Table S4 and Figure 6k,l), providing molecular-level evidence for the markedly reduced ApoE adsorption on Tc-LNPs. Given the results of the cell-based assays, protein corona analysis, and molecular dynamics simulations mentioned above, it is evident that iChol lipids, engineered to exhibit weak ApoE binding affinity, diminish ApoE/LDLR-mediated hepatic delivery through the reduction of ApoE adsorption. This, in turn, results in decreased hepatic-tropic mRNA delivery of Tc-LNPs while simultaneously promoting their extrahepatic delivery (e.g., splenic delivery).

To validate the applied ability of our design strategy across diverse ionizable lipid structures, we rationally modified the commercially available lipid ALC-0315 by replacing the branched alkyl chain (2-hexyldecanoate) with cholesterol,

https://doi.org/10.1021/jacs.5c14870
J. Am. Chem. Soc. XXXX, XXX, XXX−XXX

obtaining two cholesterol-modified variants (**i0315-AC6Chol** and **i0315-AC8Chol**, Figure S54). Molecular dynamics simulations revealed that the binding affinities between ApoE and the lipids (**i0315-AC6Chol**: −1.74; **i0315-AC8Chol**: 9.13) were weaker than those between ApoE and cholesterol (−2.02) (Table S8). Two Tc-LNPs, each incorporating one of the two ionizable lipids, were prepared for intravenous administration based on the optimized formulation. Bioluminescence analysis of harvested organs showed that **i0315-AC8Chol** Tc-LNPs achieved mRNA expression levels comparable to ALC-0315 LNPs. Notably, ALC-0315 LNPs primarily mediated hepatic mRNA expression, while Tc-LNPs, especially **i0315-AC8Chol** Tc-LNPs, exhibited splenic preference (Figure S55a). As shown in Figure S55b, **i0315-AC6Chol** and **i0315-AC8Chol** Tc-LNPs exhibited spleen-to-liver luminescence intensity ratios of 1.51 and 5.18, respectively, corresponding to 12.6-fold and 43.2-fold enhancements compared to commercial ALC-0315 LNPs (0.12). The findings indicate that employing computational-assisted rational design of lipid structures effectively minimizes ApoE adsorption on the resulting LNPs, thereby reducing hepatic accumulation and facilitating extrahepatic mRNA delivery. The strategy modulates LNP protein corona composition through structural design to achieve organ preference regulation, presenting a novel approach for LNP development.

Endosomal Escape Ability, Stability, and Biocompatibility of Tc-LNPs. We further assessed the endosomal escape efficiency, formulation stability, and biosafety of the novel cholesterol-free Tc-LNPs. Confocal microscopy analysis of HEK293 cells incubated with Tc-LNPs (Figures 7a and S56) demonstrated efficient cellular uptake and subsequent endosomal escape of ^{Cy5}mRNA-loaded Tc-LNPs (red), as evidenced by the colocalization with endosomal/lysosomal markers (green). Hemolysis assays demonstrated that Tc-LNPs showed significantly enhanced activity (up to 80% hemolysis) under acidic conditions (endosomal pH 5.0) compared to physiological pH 7.4 (Figure 7b), indicating the pH-dependent endosomal escape capability. In addition, we studied the stability of both Tc-LNPs and four-component LNPs (ALC-0315 and MC3) encapsulating luciferase mRNA following storage at 4 °C for 30 days. Tc-LNPs maintained consistent PDI, particle size, encapsulation efficiency and stability of luciferase expression in vitro and in vivo, exhibiting excellent physicochemical and functional stability, which is comparable to four-component LNP systems (Figure S57). In vitro cytotoxicity assay revealed the cell viability exceeded 95% across a wide mRNA concentration range (0.25−4 μg/mL) (Figure 7c), indicating minimal toxicity. In vivo safety assessments in Balb/c mice showed that Tc-LNP did not induce significant alterations in serum alanine aminotransferase (ALT), aspartate aminotransferase (AST), blood urea nitrogen (BUN), or creatinine (CRE) levels compared to PBS controls (Figure 7d). Furthermore, no pathological abnormalities were observed in major organs, including the heart, liver, spleen, lung, and kidney (Figure 7e). The results reveal that Tc-LNPs exhibit superior endosomal escape efficiency, robust stability, and favorable biocompatibility, highlighting their promise for clinical application.

DISCUSSION

mRNA-LNPs based therapies are heralding a new era in medicine, offering a versatile and programmable platform for the prevention and treatment of a broad spectrum of diseases.[28,38] However, LNPs predominantly accumulate in the liver following intravenous administration, thereby restricting the applications of mRNA-LNPs primarily to vaccines and liver-associated diseases.[19] The protein corona, formed by the adsorption of serum proteins, particularly ApoE, onto the surface of LNPs, plays a pivotal role in mediating their hepatic accumulation.[39] ApoE is a prototypical lipid-binding protein that interacts with cholesterol and other lipids to form lipoprotein particles, thereby regulating the transport and distribution of lipids in circulation.[40,41] Cholesterol in LNPs facilitates the adsorption of ApoE, enhancing their internalization by hepatocytes through ApoE/LDLR-mediated endocytosis.[14−16,42] The inherent liver tropism of LNPs restricts the therapeutic potential for diseases in nonhepatic organs, necessitating the development of innovative strategies to overcome delivery barriers and fully unlock the potential of mRNA-LNP-based therapies.

In this study, we introduce a strategy using molecular docking (DiffDocK-L) for the rational design of lipids in LNP formulations. We aim to reduce ApoE adsorption on LNPs, minimize hepatic accumulation, and enhance extrahepatic mRNA delivery. Using DiffDock-L, we modeled the binding conformation and affinity between cholesterol and ApoE, identifying potential interaction sites. The DiffDock-L modeling analysis suggests that phenylalanine at position 220 and leucine at position 191 of ApoE engage in van der Waals interactions with the methyl and ethyl groups, as well as the double bonds, present in rings A and B of cholesterol. (Figure 2a). To disrupt the interactions, rational modifications of the A or B ring of cholesterol, where the potential binding sites are located, are essential. Considering the need to preserve the structural integrity of cholesterol during modification, we selected the hydroxyl group on the A ring (Figure 2a) as the target for modification to induce conformational changes in cholesterol, thereby attenuating or abolishing its interactions with ApoE. To achieve an optimized LNP formulation with reduced complexity and enhanced manufacturing scalability, we integrate the ionizable center and hydrophobic alkyl chain into cholesterol through the hydroxyl group. The designed lipid is mainly divided into three parts: a hydrophilic ionizable headgroup, a hydrophobic alkyl tail, and a cholesterol alkyl tail. The lipid headgroup may comprise any of three distinct hydroxyl-conjugated tertiary amines: 4-aminobutanol, ethanolamine, or diglycolamine (Figure 3c). The amine group becomes protonated in an acidic environment, acquiring positive charges that facilitate mRNA complexation. Hydroxyl group incorporation enhances mRNA encapsulation and transfection efficiency via a synergistic mechanism mediated by electrostatic interactions and hydrogen bonding between mRNA and ionizable lipids.[43] The hydrophobic alkyl tail, comprising a branched alkyl group connected to a linear alkyl chain via a degradable linker, facilitates endosomal membrane fusion and hexagonal phase transition.[44] The cholesterol alkyl tail (Figure 3b) incorporates a cholesterol fragment conjugated to a degradable linear alkyl chain, enhances LNP stability by filling gaps between lipids and facilitates endosomal membrane fusion during cellular uptake.[45] Collectively, our computation-aided approach integrates cholesterol and the ionizable lipid-two key components of LNPs-into a single entity, facilitating the rational design of iChol lipids.

DiffDock-L simulations demonstrate that all 105 designed iChol lipids exhibit significantly lower ApoE binding affinity compared to cholesterol, validating the design strategy.

https://doi.org/10.1021/jacs.5c14870
J. Am. Chem. Soc. XXXX, XXX, XXX−XXX

Approximately 80% of iChol lipids have affinity values greater than 0 with ApoE (Figure 3d), whereas the affinity value for cholesterol is −2.02. The iChol lipids were synthesized and experimentally characterized to validate the computational predictions. All the iChol lipids can be formulated into simpler three-component LNPs (Tc-LNPs) with a narrow size distribution while maintaining transfection efficiency in vitro. The top-performing ten iChol lipids, identified based on in vitro transfection efficiency, exhibited comparable or superior in vivo efficacy compared to the commercial ALC-0315 (Figure 5a). Importantly, these Tc-LNPs (based on the ten iChol lipids) also demonstrated reduced liver tropism and enhanced mRNA delivery to extrahepatic tissues, particularly in the spleen (Figure 5f,g). Among the ten iChol lipids tested, **iChol15-C4A2** and **iChol15-C4ACM** exhibited superior transfection efficacy relative to ALC-0315 following intramuscular administration, and also achieved efficient extrahepatic mRNA delivery (Figure 5b,f). Notably, protein adsorption assays demonstrated that Tc-LNPs exhibit up to a 90% reduction in ApoE adsorption compared to conventional LNPs (Figure 6j), supporting the computation-aided design strategy. The attenuated ApoE binding reduces Tc-LNP dependence on ApoE/LDLR-mediated hepatocyte endocytosis, thereby diminishing hepatic preference. Additionally, we applied our strategy to ALC-0315 to evaluate its extensibility across different ionizable lipids. Cholesterol-modified ALC-0315 LNPs similarly demonstrated reduced hepatic accumulation without compromising transfection efficiency, validating the broad applicability of our approach. These results demonstrate that our computation-aided lipid design strategy establishes a robust framework for the rational engineering of lipids tailored for extrahepatic mRNA delivery.

It is worth noting that although both free cholesterol and ionizable lipids were replaced by iChol lipids, the stability of Tc-LNPs was not compromised. Tc-LNPs exhibited comparable stability to four-component LNPs following storage at 4 °C for 30 days, with no significant compromise in the fundamental physicochemical properties or functional performance (Figure S57). This suggests that, despite the modification altering the conformation of cholesterol, the modified cholesterol still contributes to the stability of Tc-LNPs by filling the gaps between the lipids. In addition, iChol lipids impart strong pH-mediated charge-changing properties to Tc-LNPs, promoting membrane penetration (>60% disruption at pH endosomal 5.5) and facilitating endosomal escape for efficient mRNA delivery, while exhibiting minimal effects at physiological pH (7.4). These properties enhance both the transfection efficacy and biocompatibility of Tc-LNPs. Moreover, the incorporation of biodegradable linkers into iChol lipids further improved the biocompatibility, with Tc-LNPs exhibiting no detectable cytotoxicity or adverse effects in both in vitro and in vivo at tested doses (Figure 7c−e). These results demonstrate that Tc-LNPs exhibit excellent performance for clinical translation potential.

Although the developed Tc-LNPs possess favorable properties for reducing hepatic tropism and simplifying the LNP delivery system, several aspects require further investigation. For instance, Tc-LNPs still show a certain degree of hepatic enrichment, and understanding the underlying mechanism is essential for developing next-generation Tc-LNPs with reduced liver accumulation. And the mechanism underlying spleen accumulation requires further investigation to fully understand its biological implications. Additionally, the current study was conducted in mice, future investigations should evaluate Tc-LNP distribution patterns in large animal species, including nonhuman primates, to assess the clinical translatability.

CONCLUSION

In conclusion, we have established a robust LNP platform that enables efficient extrahepatic mRNA delivery (e.g., spleen targeting) through strategic reduction of ApoE interactions, and demonstrated its capability through proof-of-concept studies. Our findings highlight the translational potential of mRNA-based therapy for diseases beyond the liver, broadening the therapeutic scope of mRNA technology.

ASSOCIATED CONTENT

Supporting Information

The Supporting Information is available free of charge at https://pubs.acs.org/doi/10.1021/jacs.5c14870.

Materials; methods; supporting schemes, tables and figures; statistical analysis (PDF)

AUTHOR INFORMATION

Corresponding Authors

Xiaoyang Xu − *Department of Chemical and Materials Engineering, New Jersey Institute of Technology, Newark, New Jersey 07102, United States; Department of Biomedical Engineering, New Jersey Institute of Technology, Newark, New Jersey 07102, United States;* orcid.org/0000-0002-1634-3329; Email: xiaoyang.xu@njit.edu

Xue-Qing Zhang − *National Key Laboratory of Innovative Immunotherapy, Shanghai Frontiers Science Center of Drug Target Identification and Delivery, School of Pharmaceutical Sciences, Shanghai Jiao Tong University, Shanghai 200240, China; Suzhou Biomedical Industry Innovation Center, Suzhou 215000, China;* orcid.org/0000-0002-4954-2586; Email: xueqingzhang@sjtu.edu.cn

Authors

Yilong Teng − *National Key Laboratory of Innovative Immunotherapy, Shanghai Frontiers Science Center of Drug Target Identification and Delivery, School of Pharmaceutical Sciences, Shanghai Jiao Tong University, Shanghai 200240, China*

Yuxuan Guo − *National Key Laboratory of Innovative Immunotherapy, Shanghai Frontiers Science Center of Drug Target Identification and Delivery, School of Pharmaceutical Sciences, Shanghai Jiao Tong University, Shanghai 200240, China*

Zhixiang Liu − *Department of Chemical and Materials Engineering, New Jersey Institute of Technology, Newark, New Jersey 07102, United States*

Maoping Tang − *National Key Laboratory of Innovative Immunotherapy, Shanghai Frontiers Science Center of Drug Target Identification and Delivery, School of Pharmaceutical Sciences, Shanghai Jiao Tong University, Shanghai 200240, China*

William Stewart − *Department of Chemical and Materials Engineering, New Jersey Institute of Technology, Newark, New Jersey 07102, United States*

Complete contact information is available at: https://pubs.acs.org/10.1021/jacs.5c14870

Author Contributions

[#]Y.L.T. and Y.X.G. contributed equally to this work.

Notes

The authors declare no competing financial interest.

■ ACKNOWLEDGMENTS

This research was funded by the National Key Research and Development Program of China (2023YFC2606003), "Open Competition to Select the Best Candidates" Key Technology Program for Nucleic Acid Drugs of NCTIB (Grant No. NCTIB2022HS02002), the Natural Science Foundation of Shanghai (23ZR1427600), and the Program of Shanghai Frontiers Science Center of Drug Target Identification and Delivery (ZXWH2170101). X.X. acknowledges support from the National Science Foundation (2001606) and the Gustavus and Louise Pfeiffer Research Foundation Award.

■ REFERENCES

(1) Adams, D.; Gonzalez-Duarte, A.; O'Riordan, W. D.; Yang, C.-C.; Ueda, M.; Kristen, A. V.; Tournev, I.; Schmidt, H. H.; Coelho, T.; Berk, J. L.; et al. Patisiran, an RNAi Therapeutic, for Hereditary Transthyretin Amyloidosis. *New Engl. J. Med* **2018**, *379* (1), 11−21.

(2) Hou, X.; Zaks, T.; Langer, R.; Dong, Y. Lipid nanoparticles for mRNA delivery. *Nat. Rev. Mater* **2021**, *6* (12), 1078−1094.

(3) Pardi, N.; Hogan, M. J.; Porter, F. W.; Weissman, D. mRNA vaccines − a new era in vaccinology. *Nat. Rev. Drug Discovery* **2018**, *17* (4), 261−279.

(4) Sahin, U.; Karikó, K.; Türeci, Ö. mRNA-based therapeutics − developing a new class of drugs. *Nat. Rev. Drug Discovery* **2014**, *13* (10), 759−780.

(5) Yonezawa, S.; Koide, H.; Asai, T. Recent advances in siRNA delivery mediated by lipid-based nanoparticles. *Adv. Drug Delivery Rev* **2020**, *154*−*155*, 64−78.

(6) Zhang, Y.; Sun, C.; Wang, C.; Jankovic, K. E.; Dong, Y. Lipids and Lipid Derivatives for RNA Delivery. *Chem. Rev* **2021**, *121* (20), 12181−12277.

(7) Zong, Y.; Lin, Y.; Wei, T.; Cheng, Q. Lipid Nanoparticle (LNP) Enables mRNA Delivery for Cancer Therapy. *Adv. Mater* **2023**, *35* (51), No. e2303261.

(8) Kim, H.; Zenhausern, R.; Gentry, K.; Lian, L.; Huayamares, S. G.; Radmand, A.; Loughrey, D.; Podilapu, A. R.; Hatit, M. Z. C.; Ni, H.; et al. Lipid nanoparticle-mediated mRNA delivery to CD34+ cells in rhesus monkeys. *Nat. Biotechnol* **2024**, 1−8.

(9) Cullis, P. R.; Felgner, P. L. The 60-year evolution of lipid nanoparticles for nucleic acid delivery. *Nat. Rev. Drug Discovery* **2024**, *23* (9), 709−722.

(10) Polack, F. P.; Thomas, S. J.; Kitchin, N.; Absalon, J.; Gurtman, A.; Lockhart, S.; Perez, J. L.; Pérez Marc, G.; Moreira, E. D.; Zerbini, C.; et al. Safety and Efficacy of the BNT162b2 mRNA Covid-19 Vaccine. *New Engl. J. Med* **2020**, *383* (27), 2603−2615.

(11) Corbett, K. S.; Edwards, D. K.; Leist, S. R.; Abiona, O. M.; Boyoglu-Barnum, S.; Gillespie, R. A.; Himansu, S.; Schäfer, A.; Ziwawo, C. T.; DiPiazza, A. T.; et al. SARS-CoV-2 mRNA vaccine design enabled by prototype pathogen preparedness. *Nature* **2020**, *586* (7830), 567−571.

(12) Akinc, A.; Querbes, W.; De, S.; Qin, J.; Frank-Kamenetsky, M.; Jayaprakash, K. N.; Jayaraman, M.; Rajeev, K. G.; Cantley, W. L.; Dorkin, J. R.; et al. Targeted Delivery of RNAi Therapeutics With Endogenous and Exogenous Ligand-Based Mechanisms. *Mol. Ther* **2010**, *18* (7), 1357−1364.

(13) Eygeris, Y.; Gupta, M.; Kim, J.; Sahay, G. Chemistry of Lipid Nanoparticles for RNA Delivery. *Acc. Chem. Res* **2022**, *55* (1), 2−12.

(14) Francia, V.; Schiffelers, R. M.; Cullis, P. R.; Witzigmann, D. The Biomolecular Corona of Lipid Nanoparticles for Gene Therapy. *Bioconjugate Chem* **2020**, *31* (9), 2046−2059.

(15) Kasiewicz, L. N.; Biswas, S.; Beach, A.; Ren, H.; Dutta, C.; Mazzola, A. M.; Rohde, E.; Chadwick, A.; Cheng, C.; Garcia, S. P.; et al. GalNAc-Lipid nanoparticles enable non-LDLR dependent hepatic delivery of a CRISPR base editing therapy. *Nat. Commun* **2023**, *14* (1), 2776.

(16) Sabnis, S.; Kumarasinghe, E. S.; Salerno, T.; Mihai, C.; Ketova, T.; Senn, J. J.; Lynn, A.; Bulychev, A.; McFadyen, I.; Chan, J.; et al. A Novel Amino Lipid Series for mRNA Delivery: Improved Endosomal Escape and Sustained Pharmacology and Safety in Non-human Primates. *Mol. Ther* **2018**, *26* (6), 1509−1519.

(17) Sebastiani, F.; Yanez Arteta, M.; Lerche, M.; Porcar, L.; Lang, C.; Bragg, R. A.; Elmore, C. S.; Krishnamurthy, V. R.; Russell, R. A.; Darwish, T.; et al. Apolipoprotein E Binding Drives Structural and Compositional Rearrangement of mRNA-Containing Lipid Nanoparticles. *ACS Nano* **2021**, *15* (4), 6709−6722.

(18) Hald Albertsen, C.; Kulkarni, J. A.; Witzigmann, D.; Lind, M.; Petersson, K.; Simonsen, J. B. The role of lipid components in lipid nanoparticles for vaccines and gene therapy. *Adv. Drug Delivery Rev* **2022**, *188*, 114416.

(19) Zhang, X.; Su, K.; Wu, S.; Lin, L.; He, S.; Yan, X.; Shi, L.; Liu, S. One-Component Cationic Lipids for Systemic mRNA Delivery to Splenic T Cells. *Angew. Chem., Int. Ed* **2024**, *63* (26), No. e202405444.

(20) Kim, J.; Eygeris, Y.; Ryals, R. C.; Jozić, A.; Sahay, G. Strategies for non-viral vectors targeting organs beyond the liver. *Nat. Nanotechnol* **2024**, *19* (4), 428−447.

(21) Saikia, S.; Bordoloi, M. Molecular Docking: Challenges, Advances and its Use in Drug Discovery Perspective. *Curr. Drug Targets* **2019**, *20* (5), 501−521.

(22) Maier, M. A.; Jayaraman, M.; Matsuda, S.; Liu, J.; Barros, S.; Querbes, W.; Tam, Y. K.; Ansell, S. M.; Kumar, V.; Qin, J.; et al. Biodegradable Lipids Enabling Rapidly Eliminated Lipid Nanoparticles for Systemic Delivery of RNAi Therapeutics. *Mol. Ther* **2013**, *21* (8), 1570−1578.

(23) Patel, S.; Ashwanikumar, N.; Robinson, E.; Xia, Y.; Mihai, C.; Griffith, J. P., III; Hou, S.; Esposito, A. A.; Ketova, T.; Welsher, K.; et al. Naturally-occurring cholesterol analogues in lipid nanoparticles induce polymorphic shape and enhance intracellular delivery of mRNA. *Nat. Commun* **2020**, *11* (1), 983.

(24) Rohner, E.; Yang, R.; Foo, K. S.; Goedel, A.; Chien, K. R. Unlocking the promise of mRNA therapeutics. *Nat. Biotechnol* **2022**, *40* (11), 1586−1600.

(25) Eberhardt, J.; Santos-Martins, D.; Tillack, A. F.; Forli, S. AutoDock Vina 1.2.0: New Docking Methods, Expanded Force Field, and Python Bindings. *J. Chem. Inf. Model* **2021**, *61* (8), 3891−3898.

(26) Koes, D. R.; Baumgartner, M. P.; Camacho, C. J. Lessons Learned in Empirical Scoring with smina from the CSAR 2011 Benchmarking Exercise. *J. Chem. Inf. Model* **2013**, *53* (8), 1893−1904.

(27) Trott, O.; Olson, A. J. AutoDock Vina Improving the speed and accuracy of docking with a new scoring function, efficient optimization, and multithreading. *J. Comput. Chem* **2010**, *31* (2), 455−461.

(28) Xiao, Y.; Tang, Z.; Huang, X.; Chen, W.; Zhou, J.; Liu, H.; Liu, C.; Kong, N.; Tao, W. Emerging mRNA technologies: Delivery strategies and biomedical applications. *Chem. Soc. Rev* **2022**, *51* (10), 3828−3845.

(29) Wu, S.; Shi, L.; Su, K.; Lin, L.; Yan, X.; Zhang, Y.; Gu, T.; Wang, Z.; Xu, T.; Liu, S. Carbonate-Bearing Ionizable Lipids for mRNA Delivery to Splenic NK Cells. *J. Am. Chem. Soc* **2025**, *147* (32), 28665−28673.

(30) O'Brien Laramy, M.; Foley, D. A.; Pak, R. H.; Lewis, J. A.; McKinney, E.; Egan, P. M.; Yerabolu, R.; Dane, E.; Dirat, O.; Saunders Gorka, L.; et al. Chemistry, manufacturing and controls strategies for using novel excipients in lipid nanoparticles. *Nat. Nanotechnol* **2025**, *20* (3), 331−344.

(31) Li, Y.; Jarvis, R.; Zhu, K.; Glass, Z.; Ogurlu, R.; Gao, P.; Li, P.; Chen, J.; Yu, Y.; Yang, Y.; et al. Protein and mRNA Delivery Enabled by Cholesteryl-Based Biodegradable Lipidoid Nanoparticles. *Angew. Chem., Int. Ed* **2020**, *59* (35), 14957−14964.

(32) Chen, J.; Xu, Y.; Zhou, M.; Xu, S.; Varley, A. J.; Golubovic, A.; Lu, R. X. Z.; Wang, K. C.; Yeganeh, M.; Vosoughi, D.; et al.

https://doi.org/10.1021/jacs.5c14870
J. Am. Chem. Soc. XXXX, XXX, XXX−XXX

Combinatorial design of ionizable lipid nanoparticles for muscle-selective mRNA delivery with minimized off-target effects. *Proc. Natl. Acad. Sci. U. S. A* **2023**, *120*, No. e2309472120.
(33) Liu, S.; Cheng, Q.; Wei, T.; Yu, X.; Johnson, L. T.; Farbiak, L.; Siegwart, D. J. Membrane-destabilizing ionizable phospholipids for organ-selective mRNA delivery and CRISPR−Cas gene editing. *Nat. Mater* **2021**, *20* (5), 701−710.
(34) Paunovska, K.; Sago, C. D.; Monaco, C. M.; Hudson, W. H.; Castro, M. G.; Rudoltz, T. G.; Kalathoor, S.; Vanover, D. A.; Santangelo, P. J.; Ahmed, R.; et al. A Direct Comparison of in Vitro and in Vivo Nucleic Acid Delivery Mediated by Hundreds of Nanoparticles Reveals a Weak Correlation. *Nano Lett* **2018**, *18* (3), 2148−2157.
(35) Jiang, K.; Tian, K.; Yu, Y.; Wu, E.; Yang, M.; Pan, F.; Qian, J.; Zhan, C. Kupffer cells determine intrahepatic traffic of PEGylated liposomal doxorubicin. *Nat. Commun* **2024**, *15* (1), 6136.
(36) Swingle, K. L.; Hamilton, A. G.; Safford, H. C.; Geisler, H. C.; Thatte, A. S.; Palanki, R.; Murray, A. M.; Han, E. L.; Mukalel, A. J.; Han, X.; et al. Placenta-tropic VEGF mRNA lipid nanoparticles ameliorate murine pre-eclampsia. *Nature* **2025**, *637* (8045), 412−421.
(37) Dilliard, S. A.; Cheng, Q.; Siegwart, D. J. On the mechanism of tissue-specific mRNA delivery by selective organ targeting nanoparticles. *Proc. Natl. Acad. Sci. U. S. A* **2021**, *118* (52), No. e2109256118.
(38) Barbier, A. J.; Jiang, A. Y.; Zhang, P.; Wooster, R.; Anderson, D. G. The clinical progress of mRNA vaccines and immunotherapies. *Nat. Biotechnol* **2022**, *40* (6), 840−854.
(39) Dalhaimer, P.; Florey, B.; Isaac, S. Interactions of Apolipoproteins with Lipid-Based Nanoparticles. *ACS Nano* **2023**, *17* (2), 837−842.
(40) Lozupone, M.; Panza, F. Impact of apolipoprotein E isoforms on sporadic Alzheimer's disease. *Neural Regen Res* **2024**, *19* (1), 80−83.
(41) Wang, H.; Kulas, J. A.; Wang, C.; Holtzman, D. M.; Ferris, H. A.; Hansen, S. B. Regulation of beta-amyloid production in neurons by astrocyte-derived cholesterol. *Proc. Natl. Acad. Sci. U. S. A* **2021**, *118* (33), No. e2102191118.
(42) Zhang, X.; Goel, V.; Robbie, G. J. Pharmacokinetics of Patisiran, the First Approved RNA Interference Therapy in Patients With Hereditary Transthyretin-Mediated Amyloidosis. *J. Clin. Pharmacol* **2020**, *60* (5), 573−585.
(43) Xue, Y.; Hou, X.; Zhong, Y.; Zhang, Y.; Du, S.; Kang, D. D.; Wang, L.; Wang, C.; Li, H.; Wang, S.; et al. LNP-RNA-mediated antigen presentation leverages SARS-CoV-2-specific immunity for cancer treatment. *Nat. Commun* **2025**, *16* (1), 2198.
(44) Buschmann, M. D.; Carrasco, M. J.; Alishetty, S.; Paige, M.; Alameh, M. G.; Weissman, D. Nanomaterial Delivery Systems for mRNA Vaccines. *Vaccines* **2021**, *9*, 65.
(45) Chaudhary, N.; Weissman, D.; Whitehead, K. A. mRNA vaccines for infectious diseases: Principles, delivery and clinical translation. *Nat. Rev. Drug Discovery* **2021**, *20* (11), 817−838.

https://doi.org/10.1021/jacs.5c14870
J. Am. Chem. Soc. XXXX, XXX, XXX−XXX